Dislocation creep of fine-grained olivine

U. H. Faul,[1] J. D. Fitz Gerald,[2] R. J. M. Farla,[2] R. Ahlefeldt,[2] and I. Jackson[2]

Received 27 November 2009; revised 1 October 2010; accepted 26 October 2010; published 11 January 2011.

[1] Deformation experiments conducted in a gas medium apparatus at temperatures from 1200 to 1350°C with a fine-grained, solution-gelation derived Fe-bearing olivine show a stress dependence of the strain rate at stresses above ~150 MPa, which is much stronger than previously reported for polycrystalline samples. The data can be fit by a power law with $\dot{\epsilon} \propto \sigma^n$ with $n \sim 7$–8, or equally well by a Peierls creep law with exponential stress dependence. Due to the observed strong stress dependence the samples deform at significantly higher strain rates at a given stress than single crystals or coarse-grained polycrystals with $n \sim 3.5$. TEM observations indicate the presence of dislocations with at least two different Burgers vectors, with free dislocations predominantly of screw character. Subgrain walls are present but are only weakly developed and have small misorientation angles. Both the rheology and dislocation structures are consistent with creep rate-limited by dislocation glide or cross slip for aggregates with grain sizes smaller than or approaching the recrystallized grain size. Deformation mechanism maps extrapolated to lithospheric temperatures using the melt-free diffusion creep rheology of Faul and Jackson (2007), the dislocation creep rheology of Hirth and Kohlstedt (2003), and the results described here indicate that deformation conditions of ultramylonitic shear zones fall near the triple point of Peierls, dislocation, and diffusion creep.

Citation: Faul, U. H., J. D. Fitz Gerald, R. J. M. Farla, R. Ahlefeldt, and I. Jackson (2011), Dislocation creep of fine-grained olivine, *J. Geophys. Res.*, *116*, B01203, doi:10.1029/2009JB007174.

1. Introduction

[2] Olivine as the most voluminous mineral in the upper mantle [e.g., *Bodinier and Godard*, 2003; *Pearson et al.*, 2003] is a key factor for understanding its rheological behavior. Since the upper mantle encompasses cold and stiff lithospheric plates, as well as adiabatic upper mantle, the rheology of olivine needs to be determined for a wide range of conditions. Four distinct deformation regimes have been identified in experiments: diffusion creep, dominating at relatively small grain size and low stress [*Cooper and Kohlstedt*, 1984; *Karato et al.*, 1986; *Hirth and Kohlstedt*, 1995a]; dislocation creep at higher stresses [*Durham and Goetze*, 1977; *Darot and Gueguen*, 1981; *Karato et al.*, 1986; *Chopra and Paterson*, 1981; *Hirth and Kohlstedt*, 1995b]; a transition region in grain size and stress between diffusion creep and dislocation creep termed dislocation-assisted grain boundary sliding [*Hirth and Kohlstedt*, 1995b, 2003]; low-temperature plasticity thought to apply at low temperatures and high stresses [*Carter and Avé Lallemant*, 1970; *Evans and Goetze*, 1979]. Experimentally determined flow laws of the respective rheologies can be used to construct deformation mechanism maps, which delineate the dominant deformation mechanism as a function of temperature, stress and grain size [*Frost and Ashby*, 1982].

[3] Seismological observation of anisotropy in the upper mantle, combined with the results of deformation experiments in the dislocation creep regime, suggest olivine deforms with a dominant slip system in the (010) crystallographic plane with a Burgers vector in the [100] direction [e.g., *Carter and Avé Lallemant*, 1970]. The rate controlling step during deformation is inferred to be climb of dislocations, which is a diffusive process [see, e.g., *Kohlstedt*, 2006]. Small amounts of water [e.g., *Katayama et al.*, 2004], pressure effects [e.g., *Mainprice et al.*, 2005] or high differential stresses may change the dominant slip system.

[4] Deformation in the dislocation creep regime leads to recrystallization, establishing a piezometric relationship between grain size and stress [*Nicolas*, 1978; *Karato et al.*, 1980; *Van der Wal et al.*, 1993; *Jung and Karato*, 2001]. Most experimental studies in the dislocation creep regime had starting grain sizes larger than the recrystallized grain size for the applied stress. The samples therefore experienced grain size reduction by recrystallization during deformation. In the experiments described here the grain size is smaller than, or approaches the recrystallized grain size at the highest stresses. The melt-free nature of the high-purity samples of this study results in a relatively high strength in diffusion creep and slower grain growth rates in comparison to melt-bearing samples [*Faul and Jackson*, 2007]. As a result, the transition from diffusion creep to dislocation creep can be observed for fine-grained samples over a range of tem-

[1]Department of Earth Sciences, Boston University, Boston, Massachusetts, USA.
[2]Research School of Earth Sciences, Australian National University, Canberra, Australian Capital Territory, Australia.

0148-0227/11/2009JB007174

Table 1. Experimental Conditions and Results, Melt-Free Samples[a]

Experiment (Total Strain, %)	T (°C)	Grain Size[b] (μm)	Grain Size[c] (μm)	Stress (MPa)	Strain Rate (s^{-1})	Strain (%)
6509	1300	5.4	5.80	**199**	**4.5×10^{-5}**	0.88
(15.6)		6.8	5.83	**221**	**7.9×10^{-5}**	1.54
			5.83	**229**	**1.1×10^{-4}**	1.04
6519	1310	4.1	4.63	145	2.2×10^{-4}	0.83
(17.2)		6.5	4.64	164	3.1×10^{-4}	0.85
			4.66	**184**	**4.8×10^{-4}**	0.87
			4.66	**201**	**7.9×10^{-4}**	1.42
			4.67	**215**	**1.3×10^{-3}**	1.83
			4.68	**227**	**2.0×10^{-3}**	1.79
			4.68	**238**	**2.8×10^{-3}**	2.49
6526	1236	4.2	4.58	163	4.2×10^{-6}	1.42
(19.3)		4.6	4.62	**202**	**8.9×10^{-6}**	3.50
			4.64	**247**	**2.5×10^{-5}**	4.25
			4.65	**291**	**6.6×10^{-5}**	3.51
6527	1185	4.4	4.84	183	1.1×10^{-6}	1.17
(18.3)		4.4[d]	4.87	**243**	**3.1×10^{-6}**	3.06
			4.88	**271**	**7.6×10^{-6}**	6.10
			4.88	**310**	**2.4×10^{-5}**	2.31
6530	1360	4.0	5.09	122	4.1×10^{-5}	1.97
(15.0)		5.5	5.12	**153**	**7.3×10^{-5}**	2.47
			5.14	**186**	**1.6×10^{-4}**	2.31
			5.14	**219**	**3.8×10^{-4}**	1.73
6532	1250	2.7	3.55	160	1.1×10^{-5}	2.17
(18.9)		4.2	3.59	**197**	**2.0×10^{-5}**	2.73
			3.62	**232**	**4.4×10^{-5}**	4.15
			3.63	**266**	**1.1×10^{-4}**	3.59

[a]This is a continuation of Table 1 of *Faul and Jackson* [2007], which contains the data used in diffusion creep fits. The confining pressure for all experiments was 300 MPa. Bold entries indicate data used for fit in equations (2) and (3).

[b]Grain size measured after hot pressing (top entry) and after deformation (bottom entry).

[c]Grain size calculated with *Faul and Jackson* [2007], equation (1) from grain size after hot pressing for half time of each constant load segment, taking the time at temperature before the beginning of deformation into account.

[d]Grain size corrected from *Faul and Jackson* [2007] by larger area EBSD mapping.

peratures. The experimental observations described below indicate that creep controlled by lattice friction (Peierls creep) occurs at small grain sizes for a wider range of conditions than previously assumed.

2. Experimental and Analytical Methods

[5] The experiments were conducted in a Paterson gas medium apparatus [*Paterson*, 1990] at a confining pressure of 300 MPa. The chief advantage of using a gas medium apparatus for triaxial compression tests is that stresses can be measured internally, and strain and strain rates can be measured directly and accurately, although the maximum total strain is limited to about 20%. Experimental methods and sample preparation are described in detail in *Faul and Jackson* [2007]. The rheology of dry, melt-free, solution-gelation (sol-gel) derived olivine, which remains fine-grained (<6 μm) at temperatures from 1200 to 1350°C (Table 1) was systematically examined for a range of differential stresses up to 310 MPa.

[6] Samples were deformed in preprogrammed segments of constant load, starting in the diffusion creep regime and continuing into the dislocation creep regime. The data for the diffusion creep regime is reported by *Faul and Jackson* [2007]. Each constant load segment was examined for steady state conditions by plotting displacement as a function of time and checking strain rates for possible initial transients from the preceding ramp in load. Table 1 contains the rheological data of those experiments that were deformed into the dislocation creep regime.

[7] Mean grain size and grain size distribution, misorientations, as well as lattice preferred orientation were obtained from Electron Backscatter Diffraction (EBSD) maps, where each pixel records the crystalline orientation at that point. EBSD maps were acquired on a Scanning Electron Microscope (SEM) with W-filament at 20 kV and nominal sample beam currents >1 nA with a minimum step size of 0.2 μm for the most fine-grained samples. At this step size the indexing rate for a conventional SEM with an older Nordif CCD camera is between 60% and 70%. The raw maps were noise reduced by first removing single pixel outliers, followed by several dilation steps. In order to avoid dilation into neighboring grains, the Euler angle maps were overlayed onto band contrast images that show grain boundaries. After the first dilation step grains less than six pixels in size were deleted since they fall below the effective mapping resolution and are not recognizable in the band contrast images.

[8] Dislocation densities were obtained by oxidizing polished sample surfaces in air for 30 min at 900°C, removal of a thin surface layer by polishing and subsequent imaging of the oxidized structures by field emission SEM (FESEM) [*Kohlstedt*, 1976; see also *Farla et al.*, 2010]. Dislocation structures were examined by TEM (transmission electron microscope operated at 300 kV) imaging of ion-thinned foils.

3. Results

3.1. Creep Equations and Fits

[9] The total strain rate during deformation is the sum of the strain rates of concurrent processes [e.g., *Poirier*, 1985]. The total strain rate $\dot{\varepsilon}_t$ can therefore be written as the sum of diffusion creep ($\dot{\varepsilon}_{diff}$) and dislocation creep ($\dot{\varepsilon}_{dis}$):

$$\dot{\varepsilon}_t = \dot{\varepsilon}_{diff} + \dot{\varepsilon}_{dis}. \quad (1)$$

The strain rate due to the diffusion creep component for the samples discussed here has been calculated from the flow law of *Faul and Jackson* [2007]. Since diffusion creep depends on grain size as $\dot{\varepsilon}_{diff} \propto d^{-3}$, uncertainties in grain size are propagated to the dislocation creep component remaining after subtraction of the diffusion creep component. In order to minimize this uncertainty, only those creep data are used for the fit of the dislocation creep component where the contribution from diffusion creep is below approximately one half log unit in strain rate (bold entries in Table 1, see Figure 1).

[10] Dislocation creep data is commonly fitted to a power law equation of the form:

$$\dot{\varepsilon}_{dis} = A_c \sigma^n \exp^{-E_c/RT}. \quad (2)$$

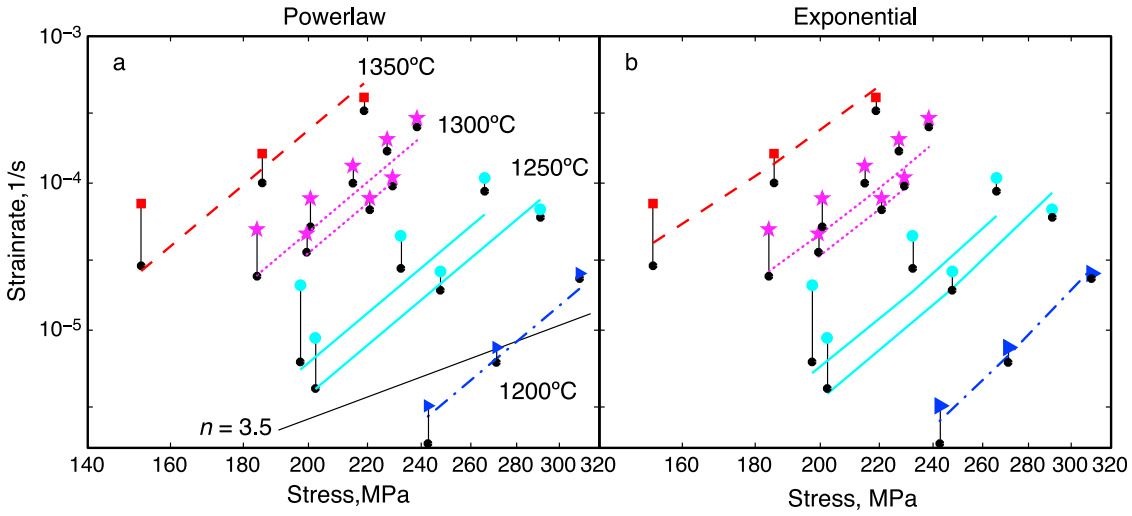

Figure 1. Fit of the bold entries in Table 1 to (a) a power law (equation (2)) and (b) an exponential creep law (equation (3)). Symbols represent the measured strain rates as given in Table 1 with black vertical lines connecting to the data after subtraction of the diffusion creep component (black dots) [*Faul and Jackson*, 2007]. Lines represent the fit to the net creep rates. Temperatures range from 1200°C (blue dash-dotted line) to 1350°C (red dashed line). The black line in Figure 1a shows a slope with $n = 3.5$. This comparison illustrates that the data can be fit equally well with either a power law or an exponential creep law.

A number of theoretical models for creep rate-limited by climb of dislocations predict $n = 3$ [e.g., *Kohlstedt*, 2006], although $n = 4.5$ can also be derived [*Poirier*, 1985]. Experimentally determined values of n for olivine range from 3.5 for polycrystalline aggregates [*Hirth and Kohlstedt*, 1995b, 2003], to values in the range from 3 to 4.5 for single crystal deformation experiments [*Bai et al.*, 1991], to 5.5 for relatively high stress deformation of polycrystalline samples [*Goetze*, 1978]. Statistical analysis of creep data from a number of different studies results in $n \approx 5$ [*Korenaga and Karato*, 2008]. Fitting of the data in Table 1 to equation (2) results in a stress exponent $n = 8.2$ with an activation energy $E_c = 682$ kJ/mol and constant $A_c = 0.3$ MPa^{-n} s^{-1} (Figure 1a).

[11] At high stresses (above 200 MPa) [*Goetze*, 1978; *Evans and Goetze*, 1979] analysis of data from single crystals points to a flow law that includes a stress dependence of the activation energy,

$$\dot{\varepsilon}_P = A_P \sigma^n \exp\left(-\frac{E_P}{RT}\left(1-\left(\frac{\sigma}{\sigma_P}\right)^p\right)^q\right) \qquad (3)$$

This flow law is inferred to apply when creep is controlled by glide of dislocations, with σ_P the resistance to glide at zero K (Peierls stress) [*Ashby and Verrall*, 1978; *Frost and Ashby*, 1982]. Theoretical considerations indicate that the exponents p and q should be in the range of $0 < p \leq 1$ and $1 \leq q \leq 2$ [*Kochs et al.*, 1975]. A stress exponent $n = 2$ can be derived with Orowan's equation, and dislocation densities related to the force balance between the applied stress and the stress field in the crystal lattice resulting from the presence of dislocations [*Poirier*, 1985]. In this model, the Peierls stress, σ_P, is proportional to the ratio h/b, where b is the Burgers vector and h the spacing of the glide planes. For metals Peierls stresses are small, but for covalently bonded materials Peierls stresses can be of order 0.1 G, where G is the shear modulus. Literature values for σ_P based on fits to equation (3) for olivine result in values in the range from 2.7 to 9.1 GPa [*Goetze*, 1978; *Evans and Goetze*, 1979; *Frost and Ashby*, 1982].

[12] The fit to the data from this study (Table 1) to equation (3) with $n = 2$ is shown in Figure 1b. Following *Evans and Goetze* [1979] we set $p = 1$ and $q = 2$. The resulting activation energy $E_P = 766 \pm 45$ kJ/mol is somewhat higher than literature values, while the Peierls stress $\sigma_P = 4200 \pm 300$ MPa falls in the range of previously reported values ($A_P = 1 \times 10^{14 \pm 1.5}$ MPa^{-n} s^{-1}). Comparison with Figure 1a shows that the data is equally well fit by equations (2) and (3). The quality of the fit cannot be improved by introducing a grain size dependence; the opx content [see *Faul and Jackson*, 2007] also produces no resolvable influence on the rheology.

[13] The combined fit ($\dot{\varepsilon}_t$, equation (1)) to both diffusion and dislocation creep is shown in Figure 2. Since the activation energies for both creep regimes are large, the stress level at which the transition between them occurs decreases only relatively slowly with increasing temperature from about 180 MPa at 1200°C to 120 MPa at 1350°C. Due to the steep increase in strain rate with stress in the dislocation creep regime the data used for the fit to the diffusion creep regime in *Faul and Jackson* [2007] does not contain significant contributions from the dislocation creep regime.

3.2. Influence of Stress and Strain on Rheology

[14] Stable dislocation structures for a given stress require a finite amount of strain. Deformation experiments with single crystal olivine indicate that dislocation density increases steeply for the first percent of strain and flattens out after about 2% [*Durham et al.*, 1977]. However, these early dislocation structures likely continue to evolve with further

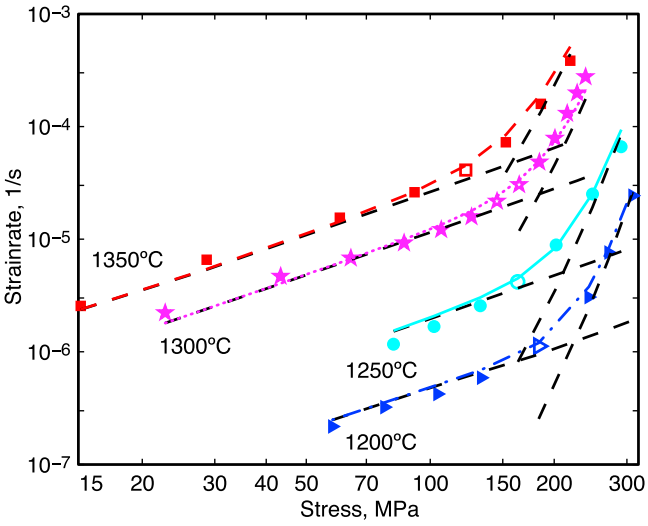

Figure 2. Creep data (same symbols as in Figure 1) and combined fit of diffusion [from *Faul and Jackson*, 2007] and exponential creep law. The data and fits range from ~15 to 300 MPa in stress, more than 3 orders of magnitude in strain rate and a temperature range of 150 K. Black dashed lines indicate diffusion and dislocation creep laws, respectively. Data points with open symbols were not included in either fit. While diffusion creep contributes significantly to the dislocation creep rheology and needs to be subtracted, due to the steep slope of the dislocation creep rheology its contribution to the data used for the fit to the diffusion creep is negligible.

strain. Insufficient strain to reach steady state dislocation structures may affect the stress dependence of the strain rate. As detailed by *Faul and Jackson* [2007] each test in this study consists of a staircase of constant load segments. Transitions between constant load segments consist of ramps in load with accelerating strain rates, which contribute to the total sample strain. The ramps are not included in Table 1.

[15] Inspection of the creep data from individual experiments in this study indicates that steady state was not reached in all cases. An example of this is shown in Figure 3a. Specimen 6526 was first deformed in an exploratory sequence of constant load segments that resulted in relatively small strains at each step, and less than 2.5% total strain in the dislocation creep regime. In the second test the strain at each step, as well as the total strain in the dislocation creep regime was significantly larger. Considering that the first constant load segment of each new sample generally exhibits a larger scatter than subsequent segments, the strain rates in the diffusion creep regime are similar in both passes. At higher stresses, however, the trends diverge, with the smaller total strain of the first test resulting in a shallower slope. Inspection of a constant load segment from the second pass with 4.26% shows no work hardening, suggesting that at this strain near steady state dislocation densities and structures were established (Figure 3b, see also TEM images of dislocation structures in section 4.2.) Samples 6509 and 6519 with strains between 1 and 2% at each constant load segment had relatively small steps in stress (10–20 MPa) between these segments.

[16] During one constant load segment of run 6527 the differential stress (310 MPa) exceeded the confining pressure (300 MPa), thus violating the "Goetze Criterion" [*Kohlstedt et al.*, 1995]. Removing this segment as well as the next highest constant load segment of 291 MPa from run 6526 from the fit does not change the flow law significantly (see also Figure 1). Published studies where the differential stress exceeds the confining pressure at high temperature (in some cases by several hundred MPa) include *Chopra and Paterson* [1981, 1984] and a study by *Rutter and Brodie* [2004] on fine-grained synthetic quartzite. The recrystallization piezometer of *Van der Wal et al.* [1993] is based on a subset of the *Chopra and Paterson* [1981, 1984] data, with differential stresses up to 421 MPa.

4. Microstructures

[17] As section 3 shows, the dislocation creep rheology of the fine-grained samples differs from that of published coarse-grained samples by its much stronger stress dependence. In order to gain insight into possible causes for this behavior, microstructural observations such as grain size distributions, lattice preferred orientation, and dislocation densities and structures are presented.

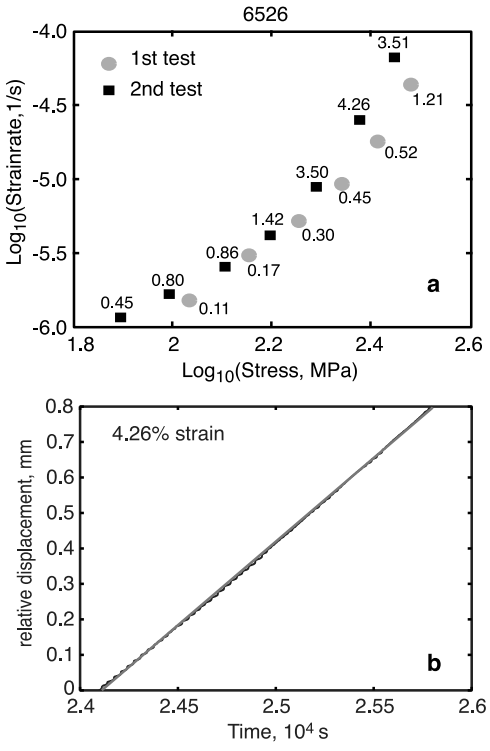

Figure 3. Influence of strain on rheology. (a) Deformation data from run 6526. Dots indicate the first, exploratory test with relatively small strains for each constant load segment (numbers next to symbols). Before the second test (squares) the stress was returned to zero. Data from the first test are not included in the fits. (b) Displacement versus time for a constant load segment of sample 6526. The data are shown in black; a linear fit is superimposed in gray.

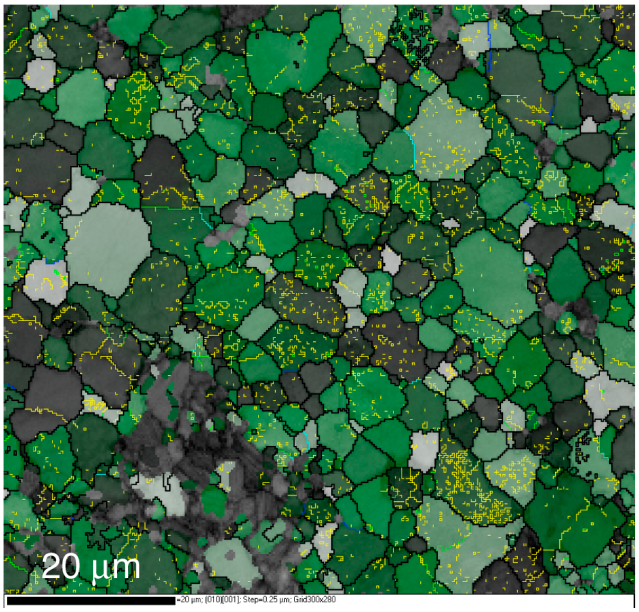

Figure 4. EBSD map of sample 6527 with a mean grain size of 4.4 μm, deformed to a total strain of 18.3% and a final flow stress of 310 MPa, the highest of this study. Green shading indicates the Schmid factor for the (010)[001] slip system, with low values displayed as black to dark green and high values as light green to white. Misorientations across boundaries are shown by colored lines, with yellow indicating misorientations 2–5°, light green 5–10°, light blue 10–20°, dark blue 20–30°, and black >30°. Continuous yellow lines indicate subgrain walls, while single pixels with small misorientations to neighbors could reflect errors in detecting the edges of the Kikuchi bands. TEM imaging (see Figures 7a and 7b) shows that some low-angle, curved subgrain walls are present in these samples. Compression direction is vertical.

4.1. Grain Scale Microstructure

[18] The effects of intragranular strain due to the imposed macroscopic deformation can be seen in EBSD maps. An example of the microstructure of the fine-grained aggregates is shown in Figure 4 (sample 6527). Most of the grains are equiaxed or only slightly elongated, with somewhat wavy grain boundaries after deformation to a total strain of 18%. This sample was deformed with a final stress of 310 MPa and shows the strong dependence of strain rate on stress detailed in section 3. EBSD maps with grain boundaries color-coded for misorientation angle show that relatively few subgrain boundaries (misorientation angle <10°) are present (Figure 4), and that recrystallized grains with small misorientation angles (<30°) are not abundant.

[19] Grain size distributions were examined after hot pressing and after deformation. For this purpose grains are defined as being completely surrounded by adjacent pixels with misorientations >10° to distinguish them from subgrains. Deformed fine-grained samples have a grain size distribution that is relatively narrow, similar to the grain size distribution after hot pressing (Figure 5).

[20] Pole figures showing the orientation of the crystal axes show no observable lattice preferred orientation in the fine-grained samples after up to 19% strain (Figure 6).

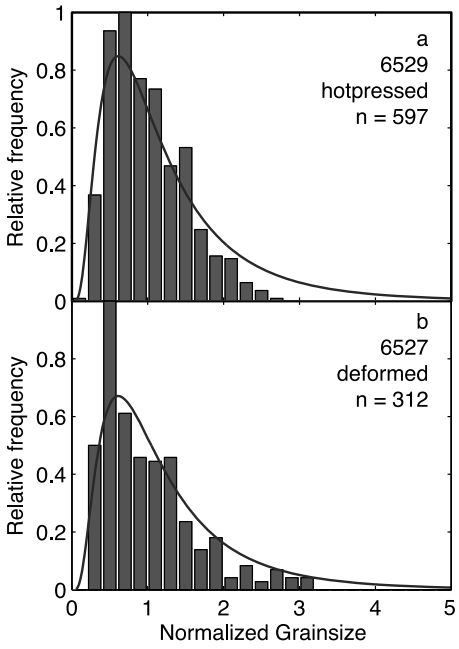

Figure 5. Histograms of grain size distributions of (a) an undeformed sample and (b) a deformed sample. Distributions are normalized by the mean grain size and the maximum of the distribution. A lognormal distribution with the same number of grains is plotted for comparison (continuous curve). The grain size distribution of the fine-grained deformed sample is not significantly broadened relative to the undeformed sample, consistent with the absence of grain size reduction by recrystallization during deformation.

Experiments where samples are deformed to larger strain are needed to determine the extent to which LPO develops in the fine-grained samples.

4.2. Dislocations

[21] Dislocation structures and densities are highly heterogenous in the deformed samples, varying both from grain

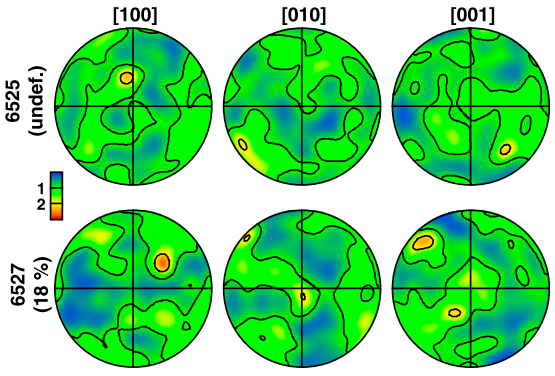

Figure 6. Lower hemisphere, equal-area pole figures showing the distribution of olivine axes after hot pressing and after deformation. Compression direction was vertical for sample 6527, deformed to 18% strain. Color scale is the same for both samples and shows multiples of uniform distribution (half width 20°, cluster size 5°).

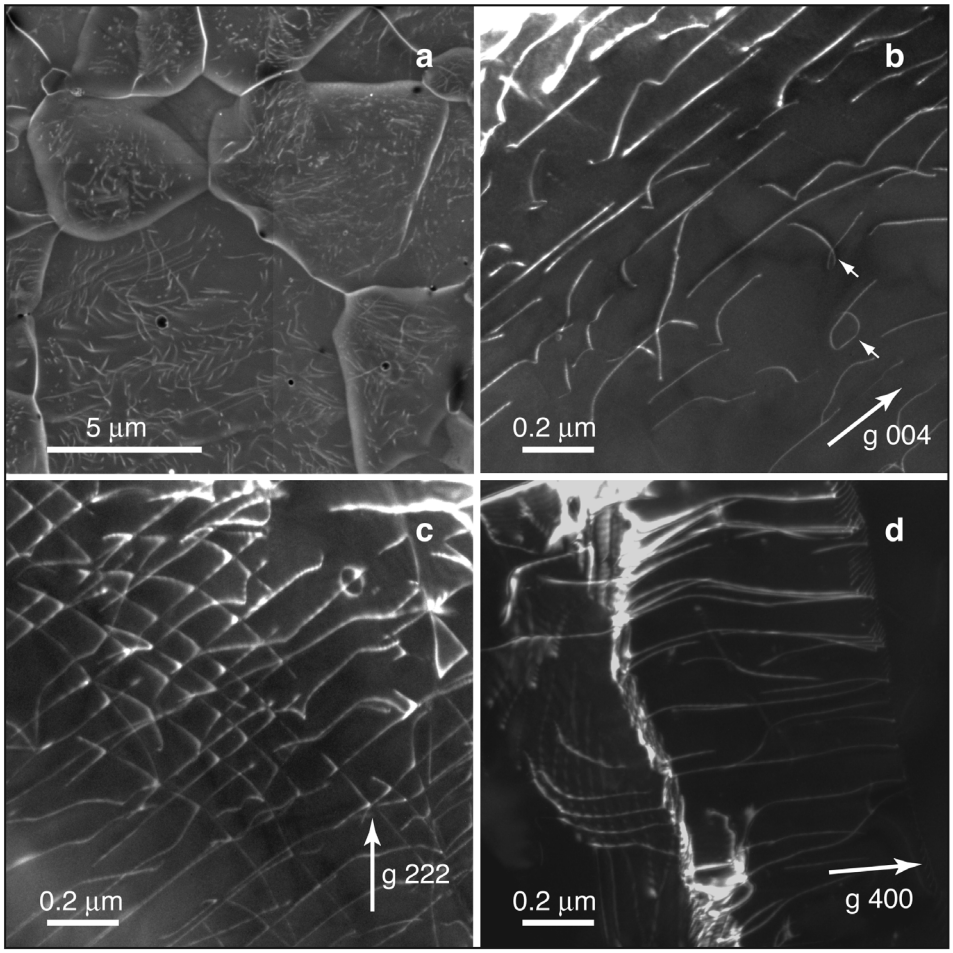

Figure 7. (a) SEM image of decorated dislocations in sample 6527. Notice the heterogeneity of the dislocation density and structure both intergranular as well as intragranular. TEM darkfield images (Figures 7b–7d) of sample 6532 showing representative dislocation structures. (b) Diffraction conditions selected to show dislocations with b = [001] Burgers vector (viewing direction near [1–10]). The dislocations have dominantly screw character with cross slip indicated by open loops (short arrows). (c) Diffraction conditions selected to show that dislocations with both b = [100] and b = [001] Burgers vector are present (viewing direction near [1–10]). Both sets of dislocations have a strong preference to lie near screw orientations. Dislocations with straight sections oriented from lower left to upper right could be pinned by orthogonal dislocations. Closed loops like the one visible near the upper right are prismatic loops (with b = [001]) left behind by moving dislocations. This arrangement of [100] and [001] Burgers vectors forms a (010) twist wall. (d) Diffraction conditions selected to show dislocations with [100] Burgers vectors (viewing direction near [001]). The subgrain wall in the center of the image consists of edge dislocations with a spacing of approximately 50 nm. Some of these edge dislocations curve away from the wall to take up near screw character with the same Burgers vector.

to grain and within individual grains (Figure 7a). A similar heterogeneity of dislocation density and intragranular strain was also noted by *Karato and Lee* [1999]. The heterogeneity of dislocation densities necessitates determination of average densities from SEM images, covering a larger area in comparison to TEM observations. Dislocations were made visible by oxidation of polished surfaces of four samples that had final stresses between 110 MPa and 310 MPa. Average dislocation densities are similar to those determined from more coarse-grained aggregates (average grain size 35 μm) [*Zhang et al.*, 2000; *Jung and Karato*, 2001] and single crystals [*Durham et al.*, 1977].

[22] Dislocation density can be related to stress as $\rho \propto \sigma^m$ [*Durham et al.*, 1977]. A fit of the data from four samples from this study results in a value of $m \sim 0.8$ (Figure 8), lower than the value of $m = 1.4$ determined by *Jung and Karato* [2001] and *Bai and Kohlstedt* [1992] and $m = 1.6$ of *Durham et al.* [1977]. Using these values for n in equation (3) above results in fits that are statistically indistinguishable from those with $m = 2$ because the stress dependence of the strain rate is dominated by the exponential factor.

[23] TEM imaging of dislocations in the fine-grained samples shows locally high dislocation densities, with many features that are similar to observations from single crystals

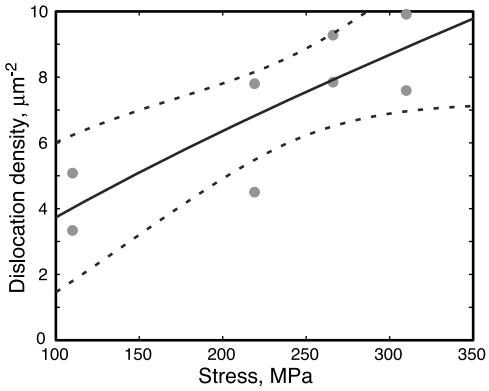

Figure 8. Dislocation density as a function of final flow stress for samples 6534 [*Faul and Jackson*, 2007], 6530, 6532, and 6527. The dislocation densities were measured on FESEM images after decorating the dislocations by oxidation (for details, see *Farla et al.* [2010]). Two separate areas were measured for each sample (dots). The data are fitted to a relation $\rho = A\sigma^m$, where ρ is the dislocation density. The solid line shows the fit, the dotted lines represent the 95% confidence interval of the fit. The resulting fit parameters are $A = 0.11$ MPa^{-m} μm^{-2} and $m = 0.77$.

[e.g., *Durham et al.*, 1977; *Darot and Gueguen*, 1981; *Bai and Kohlstedt*, 1992]. Free dislocations commonly have mixed character, but are dominated by straight screw segments (Figure 7b). Cross slip of [001] screw dislocations (Figure 7b), as well as sessile dislocation loops are also observed (Figure 7c). Burgers vectors appear to be about equally partitioned between [100] and [001] (Figure 7c) [cf. *Durham et al.*, 1977, Figures 2c and 2d] similar to observations from deformed San Carlos olivine [*Karato et al.*, 1986; *Jung et al.*, 2006], Anita Bay Dunite [*Doukhan et al.*, 1984] and natural samples [*Goetze and Kohlstedt*, 1973].

[24] Subgrain walls are generally not organized into well defined, planar structures as is observed for deformed single crystals [cf., *Durham et al.*, 1977; *Bai and Kohlstedt*, 1992]. They tend to appear irregular in shape, frequently with relatively large dislocation spacing so that the resulting misorientation is small (generally <1°). Figure 7d shows a subgrain wall formed by [100] edge dislocations with some dislocations curving away from the wall to take up near screw character. This type of arrangement was termed "[100]-organization" by *Durham et al.* [1977, Figures 3e and 3f]. Less common is the type of arrangement shown in Figure 7c where both [100] and [001] dislocations lie in near screw orientations and form irregular, low-angle wall structures of (010) twist geometry. This arrangement is again observed in deformed single crystals [*Durham et al.*, 1977; *Bai and Kohlstedt*, 1992].

5. Comparison With Previous Studies

[25] In the diffusion creep regime the experiments detailed by *Faul and Jackson* [2007] indicate that small amounts of melt have a substantial influence on creep strength. This is illustrated in Figure 9 which shows that the samples of *Mei and Kohlstedt* [2000] with grain sizes from 15 to 18 μm and up to 1% melt have a similar strength as melt-free sol-gel olivine with a grain size of 4 μm. The effect of melt on dislocation creep is expected to be less significant, since this creep mechanism involves intragranular processes.

[26] Beyond the diffusion creep regime the samples of *Mei and Kohlstedt* [2000] show no obvious grain size dependence for grain sizes ranging from 15 to 18 μm (where given). *Korenaga and Karato* [2008] also did not include a grain size dependence (except for diffusion creep) in their fit to the data shown here. The dry, nominally melt-free data of *Hirth and Kohlstedt* [1995a] with a grain size range from ~10 to 18 μm plot near the combined constitutive relation for melt-free diffusion creep, dislocation creep and (grain size dependent) dislocation-accommodated grain boundary sliding of *Hirth and Kohlstedt* [2003] (dashed line, their equation (7)), calculated for a grain size of 16 μm. The sample from *Karato et al.* [1986] with a final grain size of 18 μm plots neat the exponential creep law. Overall this group of data does not show a consistent grain size dependence, which is indicated by the difficulty in using the flow laws of *Hirth and Kohlstedt* [2003] to normalize grain size-dependent components of the data.

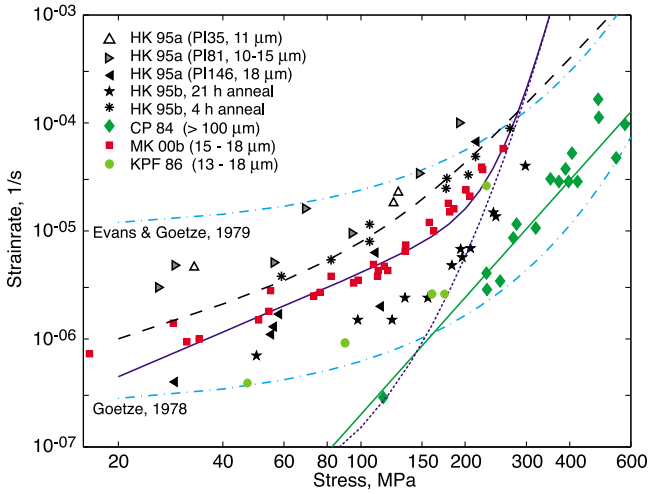

Figure 9. Comparison of creep data and fits at 1250°C. All data are plotted as reported since grain size information is only partially available: red squares [*Mei and Kohlstedt*, 2000]; triangles [*Hirth and Kohlstedt*, 1995a]; asterisks, stars [*Hirth and Kohlstedt*, 1995b]; light green circles [*Karato et al.*, 1986]. Green diamonds and green line (n = 3.6) represent data and fit from *Chopra and Paterson* [1984] from cored natural dunites (dried samples, strain rates recalculated from 1210 and 1300°C with their activation energy of 535 kJ/mol). Blue solid line shows combined melt-free diffusion and exponential creep flow law from this study for a grain size of 4 μm; short dashed for a grain size of 16 μm. Dashed black line shows the combined diffusion, dislocation, and dislocation accommodated grain boundary sliding law from *Hirth and Kohlstedt* [2003] (equation (7)) for a grain size of 16 μm. The dash-dotted light blue lines show exponential creep laws given by *Evans and Goetze* [1979] and *Goetze* [1978]. Relatively fine-grained samples (less than about 20 μm) plot to the left of the short-dashed exponential creep curve.

[27] *Hirth and Kohlstedt* [1995b] group their dry, nominally melt-free samples into those with a hot pressing time of 4 h (more fine-grained) and a hot pressing time of 21 h (more coarse-grained) [*Hirth and Kohlstedt*, 1995b]. Only grain size histograms of two samples are given, the data is therefore shown as reported. The more fine-grained samples plot between the data from *Hirth and Kohlstedt* [1995a] and *Mei and Kohlstedt* [2000], while the more coarse-grained samples plot between the exponential creep law and the creep law of *Chopra and Paterson* [1981, 1984]. Their cored natural samples contain melt at the experimental temperatures, but its distribution is highly heterogeneous [cf. *Doukhan et al.*, 1984; *Aizawa et al.*, 2008]. These samples have a (mean) initial grain size of 0.1 mm (Anita Bay dunite) and 0.9 mm (Aheim Dunite). The strain rates of the (dry) data of *Chopra and Paterson* [1984] have been recalculated to 1250°C with their activation energy and fall near their flow law (solid line) with $n = 3.6$.

[28] Figure 9 indicates that samples with grain sizes smaller than about 20 μm at stresses above 150–200 MPa do not exceed the strength given by the exponential flow law. However, there are few data from fine-grained samples at the highest stresses. Most of these data also fall near the transition from diffusion creep to dislocation creep, making it difficult to isolate the stress exponent in the dislocation creep regime. This may have obscured a stronger stress sensitivity of strain rate (see section 6.1 below) [*Mitchell et al.*, 2002].

6. Discussion

[29] This section examines possible models for the rheology of the fine-grained samples presented above. First some results from other minerals are discussed (section 6.1), followed by a summary of dislocation structures (section 6.2) and possible rheological models for the strong stress dependence observed here (section 6.3). In section 6.4 possible reasons for the difference in behavior of the more coarse-grained samples are discussed (section 6.4).

6.1. High Stress Exponents in Minerals

[30] Experimental deformation of calcite has yielded a much broader range of flow behavior than thus far observed for olivine. Besides diffusion creep and power law creep, a regime where the strain rate depends exponentially on stress has long been recognized [*Rutter*, 1974; *Schmid et al.*, 1980; *Pieri et al.*, 2001; *Renner et al.*, 2002]. *Renner and Evans* [2002] emphasize that there is no interval in stress where the (apparent) stress exponent $n' = \partial \ln \dot{\varepsilon} / \partial \ln \sigma$, fitted to a power law creep equation such as equation (2), is constant. They find that the stress exponent systematically increases with increasing stress, similar to the behavior we report here for fine-grained olivine.

[31] *Mitchell et al.* [2002] show that this behavior derives naturally from an exponential flow law, such as equation (3). They assume a model of double kink nucleation and propagation on dislocations of materials with high Peierls stress as the underlying physical process. For calcite the physical process has not been unambiguously identified, but suggestions include jogged screw dislocation models, dislocation cross slip and glide models [*Renner and Evans*, 2002]. A difference to olivine may be that the (apparent) stress exponent n' varies with grain size for calcite. *Renner and Evans* [2002] find that n' increases with increasing grain size (their Figure 2b), although this may not apply for grain sizes <10 μm [*Barnhoorn et al.*, 2004]. For olivine Figure 9 shows that more coarse-grained aggregates may have a smaller (and apparently constant) stress sensitivity in comparison to fine-grained aggregates.

[32] For olivine, stress exponents $n > 3.5$ have also been reported from deformation experiments with a solid confining medium [e.g., *Carter and Avé Lallemant*, 1970, $n \sim 5$]. However, *Kirby and Raleigh* [1973] noted, due to subsequent improvements in sample-assembly design, that indications existed for olivine to deform with a lower value of n, approximately 3.

6.2. Dislocation Character and Slip Systems in Olivine

[33] A slip system consists of slip plane and slip direction, the latter given by the Burgers vector. While Burgers vectors of individual dislocations can be determined using TEM, the corresponding slip planes cannot be readily determined. These are therefore determined in experiments with single crystals, which are deformed in orientations that favor the dominant slip systems [e.g., *Durham and Goetze*, 1977; *Darot and Gueguen*, 1981; *Bai et al.*, 1991; *Raterron et al.*, 2009]. Although the (010) plane is identified as the dominant slip plane of olivine, others (of type {0kl}) have been observed, both optically and by TEM [*Raleigh*, 1968; *Carter and Avé Lallemant*, 1970; *Phakey et al.*, 1972; *Durham et al.*, 1977; *Cordier*, 2002; see also *Tommasi et al.*, 2000]. *Durinck et al.* [2007] have analyzed a similar range of slip systems with ab initio modeling of dislocation structures, including [100](021).

[34] In contrast to deformed single crystals, in polycrystalline aggregates constraints from neighboring grains result in heterogeneous stresses and operation of several slip systems within individual grains [*Phakey et al.*, 1972, p. 136; *Karato and Lee*, 1999]. This is consistent with the observed heterogenous intragranular dislocation density and structure and identification of two different Burgers vectors. Simultaneous operation of more than one slip system with different slip planes, as well as grain boundary sliding (see below), may be the cause for the slow development of lattice preferred orientation (LPO) for the fine-grained samples (Figure 6).

[35] The majority of free dislocations have dominantly screw character (Figure 7) with long straight segments. Computer simulations of the atomic structure of [001] screw dislocations predict a core that is spread over several planes [*Carrez et al.*, 2008]. This effect could control the line direction and restrict mobility of the dislocations. Relatively long, straight dislocation segments (cf. Figure 7b) are consistent with deformation by dislocation glide for materials with a relatively high Peierls stress [e.g., *Karato*, 2008].

6.3. Grain Boundary Sliding

[36] Grain boundary sliding, commonly invoked to explain the absence of grain shape change during deformation in the diffusion creep regime [*Ashby and Verrall*, 1973], may also contribute strain at higher stresses in the dislocation creep regime [e.g., *Langdon*, 1994]. Microstructural characteristics of grain boundary sliding include, besides the absence of grain flattening, also the presence of numerous four-grain

junctions [e.g., *Goldsby and Kohlstedt*, 2001]. Microstructural models of dislocation-accommodated grain boundary sliding predict a grain size exponent $p = 1$ and a stress exponent $n = 3$ for grains that are larger than the subgrain size [*Langdon*, 1994]. At grain sizes smaller than the subgrain size, exponents of $p = 2$ and $n = 2$ are predicted to explain superplastic creep in metals at small grain sizes, where large strains are achieved without macroscopic fracture in tensile deformation. In the model proposed by *Langdon* [1994, 2006] the (rate controlling) accommodation mechanism for sliding involves extrinsic (grain boundary) dislocations, as well as dislocations forming subgrain boundaries. The salient aspect of this model is that the transition to superplastic behavior occurs when the grain size is smaller than the subgrain size. In this case dislocation pileups occur at two-grain boundaries instead of subgrain triple junctions.

[37] Comparison of the assumptions and predictions of models for grain boundary sliding with observations from our deformed samples show a number of differences. The most significant difference is that the stress exponent observed in this study is much higher than model predictions for grain boundary sliding of 1–3 [see also *Poirier*, 1985; *Karato*, 2008]. Similarly, no grain size dependence is observed for the fine-grained samples of this study, in contrast to model predictions. Examination of band contrast images, as well as SEM images of decorated surfaces indicates that four-grain junctions (a consequence of neighbor switching during grain boundary sliding) are not more numerous in deformed samples than in hot-pressed samples, where they are presumably due to grain growth.

[38] A key aspect of the model of *Langdon* [1994] is the treatment of grain boundary dislocations. To the best of our knowledge, no grain boundary dislocations have ever been imaged in natural or synthetic olivine polycrystals. While dislocations in low-angle subgrain walls are routinely imaged using TEM [e.g., *Goetze and Kohlstedt*, 1973; *Ricoult and Kohlstedt*, 1983], the only boundaries to show dislocation features at somewhat larger angles are tilt boundaries with misorientations up to 21.5° [*Heinemann et al.*, 2005; *Drury and Pennock*, 2007]. A periodic strain contrast sometimes reported has a repeat distance of ~100 nm, too large to be associated with dislocation structures, as confirmed by lattice imaging [*Heinemann et al.*, 2005]. General high-angle, olivine-olivine grain boundaries with arbitrary misorientations are imaged as ~1 nm wide regions lacking any strain contrast to indicate the presence of dislocations [e.g., *de Kloe et al.*, 2000; *Faul et al.*, 2004]. However, these grain boundary regions are known to be enriched in incompatible elements [*Drury and Fitz Gerald*, 1996; *Hiraga et al.*, 2003]. They are expected to act as sources [e.g., *Hull and Bacon*, 1984] or sinks for lattice dislocations moving through the adjacent crystals.

[39] *Hirth and Kohlstedt* [1995b] observed a nonlinear but grain size-dependent rheology at the transition from diffusion to dislocation creep. They inferred grain boundary sliding as strain producing mechanism to explain the larger than expected influence of melt on the rheology. *Hirth and Kohlstedt* [2003] proposed dislocation-accommodated grain boundary sliding as a deformation mechanism also for nominally melt-free samples with reference to *Langdon* [1994], although the combination of $p = 2$ with $n = 3.5$ cannot be directly linked to one of the above microstructural models.

[40] Grain boundary sliding may occur in our samples as a consequence of the small grain size. Grain boundary sliding would also be consistent with the absence (or slow development) of LPO and lack of grain flattening. In this view, while grain boundary sliding is the strain producing mechanism, the accommodating and rate-limiting step would be dislocation glide and cross slip involving more than one slip system (within individual grains as well as for grains of different orientations), resulting in the observed exponential stress dependence without grain size sensitivity.

6.4. Transition to Larger Grain Sizes

[41] Coarse-grained samples deformed in the dislocation creep regime show a reduction in grain size due to dynamic recrystallization [*Karato et al.*, 1986; *Van der Wal et al.*, 1993; *Zhang et al.*, 2000; *Bystricky et al.*, 2000]. The microstructure in this case consists of large relict porphyroclasts and small recrystallized grains (core and mantle structure [e.g., *Lee et al.*, 2002]). Porphyroclasts remain even after strains as large as $\gamma \sim 5$ [*Bystricky et al.*, 2000]. The recrystallized grain size is observed to be linearly dependent on stress [*Karato et al.*, 1980; *Van der Wal et al.*, 1993; *Jung and Karato*, 2001; *De Bresser et al.*, 2001] but independent of temperature [*Drury*, 2005]. For differential stresses between 200 and 300 MPa the recrystallized grain size should range from 10 to 5.5 μm, respectively [*Van der Wal et al.*, 1993]. The grain sizes of the fine-grained samples in this study are therefore at or below the predicted recrystallized grain size (Table 1), consistent with the microstructural observations (Figure 4, see section 4 above). Grain growth rates for the sol-gel samples have been determined by *Faul and Jackson* [2007] from samples deformed in the diffusion creep regime only. These observations indicate that the grain size changes very little due to growth during the relatively short duration of deformation in the dislocation creep regime (Table 1).

[42] We propose the following link between deformation mechanisms and grain size: With increasing stress at small grain sizes accommodation of grain boundary sliding switches from diffusion to dislocation motion, with a corresponding transition in rheology. For grain sizes exceeding the subgrain size/recrystallized grain size dislocations can no longer glide freely into grain boundaries, but become pinned by dislocations of a different Burgers vector (Figure 7c), or form arrays of dislocations of the same Burgers vector (Figure 7d). For sufficiently large strain and grain size these structures become organized into subgrain walls. Rate control by climb of edge dislocations (dominating subgrain walls) is consistent with the rheology observed for coarse-grained samples. To better constrain the role of subgrain boundaries for the transition from the behavior seen in fine-grained samples (<20 μm) to that in samples with grain sizes >100 μm experiments with intermediate grain sizes are needed.

7. Implications for Lithospheric Shear Zones

[43] Ultramylonites in shear zones have been described both for ophiolites [*Vissers et al.*, 1995; *Newman et al.*, 1999; *Michibayashi and Mainprice*, 2004] as well as abyssal peridotites [*Warren and Hirth*, 2006]. Common observations are the ultrafine grain size (<10 μm), near equiaxed grains with relatively straight grain boundaries, weak or lack of lattice

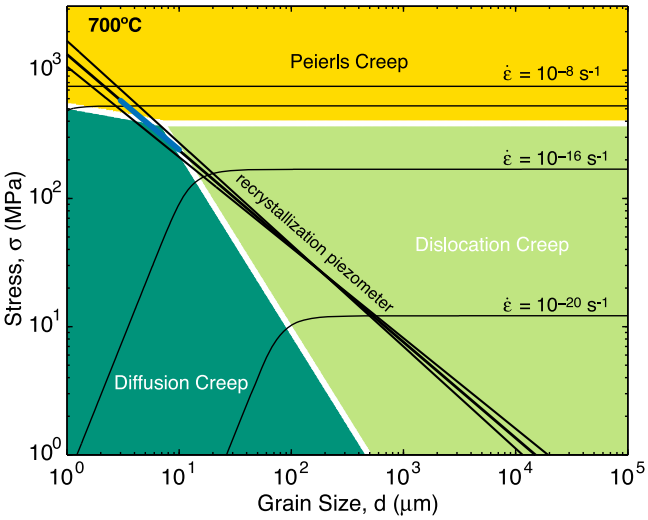

Figure 10. Deformation mechanism map calculated for 700°C [see *Warren and Hirth*, 2006, Figure 5a]. Field boundaries are based on flow laws from this study (Peierls creep), *Faul and Jackson* [2007] (diffusion creep), and *Hirth and Kohlstedt* [2003] (dislocation creep). Due to the strength of the melt-free diffusion creep rheology of *Faul and Jackson* [2007], the recrystallized grain size falls predominantly in the dislocation creep regime at this temperature, in contrast to the fields calculated with the rheology for nominally melt-free olivine [*Hirth and Kohlstedt*, 2003; *Warren and Hirth*, 2006]. The grain sizes and stresses estimated for an abyssal ultramylonite by *Warren and Hirth* [2006] are indicated by the blue bar, highlighting that deformation conditions for ultramylonites fall near the join of all three creep mechanisms. The recrystallization piezometer was determined for olivine experimentally deformed under dry conditions [*Karato et al.*, 1980; *Van der Wal et al.*, 1993].

preferred orientation and lack of signs of intragranular plastic deformation such as subgrain boundaries [*Vissers et al.*, 1995]. The lack of lattice preferred orientation and fine grain size are usually used to infer diffusion creep as dominant deformation mechanism, even though deformation in a shear zone occurs at relatively high strain rates (10^{-14} to 10^{-10} s^{-1}), [e.g., *Warren and Hirth*, 2006] but low temperatures (600–1000°C).

[44] Samples of a low-temperature shear zone from the Hilti mantle section of the Oman ophiolite exhibit a decreasing fabric intensity with increasing mylonitization and accompanying grain size reduction [*Michibayashi and Mainprice*, 2004]. The most fine-grained and highly deformed sample in their study had a random LPO pattern. In the most fine-grained portions of an oceanic peridotite mylonite with grain sizes from 3 to 10 μm, similar to this study, stresses estimated with the recrystallization piezometer range from 240 to 580 MPa [*Warren and Hirth*, 2006]. This most fine-grained part of the sample had no LPO [*Warren and Hirth*, 2006] therefore inferred that diffusion creep was dominating the rheology. The coarser-grained portions had a lattice preferred orientation consistent with operation of the (010)[100] slip system, with the strength of the LPO decreasing with decreasing grain size. An additional factor for the strength of LPO may, however, be the presence of secondary phases such as orthopyroxene.

[45] The rheology for the dry, trace element- and melt-free sol-gel olivine is illustrated in the deformation mechanism map in Figure 10. It incorporates the diffusion creep rheology determined by *Faul and Jackson* [2007], the Peierls creep parameters from this study, and the dry dislocation creep parameters from *Hirth and Kohlstedt* [2003]. Due to the increased strength in the diffusion creep regime of the melt-free samples, the diffusion creep field shrinks significantly in comparison to the nominally melt-free rheology. As a consequence, at 700°C the recrystallization piezometer falls mostly in the dislocation creep field, rather than the diffusion creep field [cf. *Warren and Hirth*, 2006, Figure 5a]. The transition to Peierls creep ("low-temperature plasticity") occurs at similar stresses for diffusion creep and dislocation creep. At the relatively high stresses inferred from the piezometric grain size for the ultramylonites, deformation occurs in the Peierls creep regime at grain sizes below about 5 μm, and near the triple point between Peierls creep, diffusion creep and dislocation creep at grain sizes up to 10 μm. With the parameters for Peierls creep given by *Goetze* [1978] the diffusion creep field expands slightly relative to the Peierls creep field, but the transition to Peierls creep from dislocation creep is similar as for the fine-grained rheology. At lower stresses/larger recrystallized grain size deformation occurs increasingly in the dislocation creep regime, consistent with the increasing strength of the lattice preferred orientation observed [e.g., *Michibayashi and Mainprice*, 2004; *Warren and Hirth*, 2006].

[46] While grain size reduction by recrystallization occurs in the dislocation creep regime at coarser grain sizes, an component for strain localization in shear zones may be that the recrystallized grain size falls near the field boundary to grain size-dependent diffusion creep [see also *De Bresser et al.*, 2001]. With grain growth rates determined by *Faul and Jackson* [2007] for melt-free, dry olivine, growth to 10 μm at 700°C requires about 1 Ma, so that no secondary phases are required to pin the grain size at the recrystallized grain size.

8. Conclusions

[47] Deformation of fine-grained sol-gel olivine shows a dependence of strain rate on stress that is significantly larger than predicted by models of dislocation creep rate-limited by climb. The data can be fitted to an exponential creep law that is predicted for creep by dislocation glide or cross slip. Examination of free dislocations show that the fine-grained aggregates have dislocations with Burgers vectors, densities and structures comparable to coarse-grained samples and single crystals, but lack evidence for rotation recrystallization, such as well-developed subgrain walls and common low angle grain boundaries. The lack of coherent subgrain walls suggests that, at sufficiently small grain sizes, many dislocations are captured by grain boundaries, leaving relatively few organized subgrain walls, characteristic of deformed single crystals and natural coarse-grained olivine. The rheology of fine-grained aggregates is therefore rate-limited by dislocation glide, while that of coarse-grained aggregates is rate-limited by climb of dislocations in subgrain boundaries. The increased creep strength of the pure sol-gel materials

relative to nominally melt-free olivine will need to be confirmed for materials that contain trace amounts of CaO and Al_2O_3, similar to natural olivine, but no melt.

[48] Construction of a deformation mechanism map with the rheology determined from melt-free sol-gel olivine for both diffusion creep and Peierls creep, together with the rheology observed for coarse-grained olivine in dislocation creep suggests a significantly reduced field for diffusion creep. Due to the increased strength in diffusion creep the grain size predicted by recrystallization piezometers falls into the dislocation creep field for grain sizes >10 μm, rather than the diffusion creep field as for nominally melt-free olivine. Deformation conditions inferred for ultramylonites in shear zones at temperatures just above the brittle-ductile transition fall near the field boundary between diffusion and dislocation creep, extending into the Peierls creep field for the highest stresses. The involvement of grain size-sensitive diffusion creep enables localization of deformation in these shear zones. For deformation at coarser grain sizes in the upper mantle a power law with $n \sim 3.5$ is expected to apply.

[49] **Acknowledgments.** Discussions with Shun Karato are gratefully acknowledged. Reviews by Greg Hirth and Bill Durham helped to improve the manuscript. We thank Harri Kokkonen for help with sample preparation and Frank Brink for help with the scanning electron microscopy. We also thank Jessica Warren for providing the scripts to calculate the deformation mechanism map.

References

Aizawa, Y., A. Barnhoorn, U. H. Faul, J. D. Fitz Gerald, I. Jackson, and I. Kovacs (2008), Seismic properties of Anita Bay dunite: An exploratory study of the influence of water, *J. Petrol.*, *49*, 841–855, doi:10.1093/petrology/egn007.

Ashby, M. F., and R. A. Verrall (1973), Diffusion accommodated flow and superplasticity, *Acta Metall.*, *21*, 149–163, doi:10.1016/0001-6160(73)90057-6.

Ashby, M. F., and R. A. Verrall (1978), Micromechanisms of flow and fracture, and their relevance to the rheology of the upper mantle, *Philos. Trans. R. Soc. London, Ser. A*, *288*, 59–95, doi:10.1098/rsta.1978.0006.

Bai, Q., and D. L. Kohlstedt (1992), High-temperature creep of olivine single crystals: 2. Dislocation structures, *Tectonophysics*, *206*, 1–29, doi:10.1016/0040-1951(92)90365-D.

Bai, Q., S. J. Mackwell, and D. L. Kohlstedt (1991), High-temperature creep of olivine single crystals: 1. Mechanical results for buffered samples, *J. Geophys. Res.*, *96*(B2), 2441–2463, doi:10.1029/90JB01723.

Barnhoorn, A., M. Bystricky, L. Burlini, and K. Kunze (2004), The role of recrystallisation on the deformation behaviour of calcite rocks: Large strain torsion experiments on Carrara marble, *J. Struct. Geol.*, *26*, 885–903, doi:10.1016/j.jsg.2003.11.024.

Bodinier, J.-L., and M. Godard (2003), Orogenic, ophiolitic and abyssal peridotites, in *Treatise on Geochemistry*, vol. 2, edited by R. W. Carlson, pp. 103–170, Elsevier, Amsterdam.

Bystricky, M., K. Kunze, L. Burlini, and J.-P. Burg (2000), High shear strain of olivine aggregates: Rheological and seismic consequences, *Science*, *290*, 1564–1567, doi:10.1126/science.290.5496.1564.

Carrez, P., A. M. Walker, A. Metsue, and P. Cordier (2008), Evidence from numerical modeling of 3d spreading of [001] screw dislocations in Mg2SiO4 forsterite, *Philos. Mag.*, *88*, 2477–2485, doi:10.1080/14786430802363804.

Carter, N. L., and H. G. Avé Lallemant (1970), High temperature flow of dunite and peridotite, *Geol. Soc. Am. Bull.*, *81*, 2181–2202, doi:10.1130/0016-7606(1970)81[2181:HTFODA]2.0.CO;2.

Chopra, P. N., and M. S. Paterson (1981), The experimental deformation of dunite, *Tectonophysics*, *78*, 453–473, doi:10.1016/0040-1951(81)90024-X.

Chopra, P. N., and M. S. Paterson (1984), The role of water in the deformation of dunite, *J. Geophys. Res.*, *89*(B9), 7861–7876, doi:10.1029/JB089iB09p07861.

Cooper, R. F., and D. L. Kohlstedt (1984), Solution-precipitation enhanced diffusional creep of partially molten olivine-basalt aggregates during hot-pressing, *Tectonophysics*, *107*, 207–233, doi:10.1016/0040-1951(84)90252-X.

Cordier, P. (2002), Dislocations and slip systems of mantle minerals, in *Plastic Deformation of Minerals and Rocks*, *Rev. Mineral. Geochem.*, vol. 51, edited by S. I. Karato and H. R. Wenk, pp. 137–179, Mineral. Soc. of Am., Washington, D. C.

Darot, M., and Y. Gueguen (1981), High-temperature creep of forsterite single crystals, *J. Geophys. Res.*, *86*(B7), 6219–6234, doi:10.1029/JB086iB07p06219.

De Bresser, J. H. P., J. H. Ter Heege, and C. J. Spiers (2001), Grain size reduction by dynamic recrystallization: Can it result in major rheological weakening?, *Int. J. Earth Sci.*, *90*, 28–45, doi:10.1007/s005310000149.

de Kloe, R., M. R. Drury, and H. L. M. van Roermund (2000), Evidence for stable grain boundary melt films in experimentally deformed olivine-orthopyroxene rocks, *Phys. Chem. Miner.*, *27*, 480–494, doi:10.1007/s002690000090.

Doukhan, N., J. C. Doukhan, J. D. Fitz Gerald, P. N. Chopra, and M. S. Paterson (1984), A TEM microstructural study of experimentally deformed anita bay dunite, in *Deformation of Ceramic Material II*, vol. 18, edited by R. E. Tressler and R. C. Bradt, pp. 307–319, Plenum, New York.

Drury, M., and G. M. Pennock (2007), Subgrain rotation recrystallization in minerals, *Mater. Sci. Forum*, *550*, 95–104, doi:10.4028/www.scientific.net/MSF.550.95.

Drury, M. R. (2005), Dynamic recrystallization and strain softening of olivine aggregates in the laboratory and the lithsophere, in *Deformation Mechanisms, Rheology and Tectonics: From Minerals to the Lithsophere*, edited by D. Gapais, J. P. Brun, and P. R. Cobbold, *Geol. Soc. Spec. Publ.*, 243, 143–158.

Drury, M. R., and J. D. Fitz Gerald (1996), Grain boundary melt films in upper mantle rocks, *Geophys. Res. Lett.*, *23*(7), 701–704, doi:10.1029/96GL00702.

Durham, W. B., and C. Goetze (1977), Plastic flow of oriented single crystals of olivine: 1. Mechanical data, *J. Geophys. Res.*, *82*(36), 5737–5753, doi:10.1029/JB082i036p05737.

Durham, W. B., C. Goetze, and B. Blake (1977), Plastic flow of oriented single crystals of olivine: 2. Observations and interpretations of dislocation structures, *J. Geophys. Res.*, *82*(36), 5755–5770, doi:10.1029/JB082i036p05755.

Durinck, J., P. Carrez, and P. Cordier (2007), Application of the Peierls-Nabarro model to dislocations in forsterite, *Eur. J. Mineral.*, *19*, 631–639, doi:10.1127/0935-1221/2007/0019-1757.

Evans, B., and C. Goetze (1979), The temperature variation of hardness of olivine and its implications for polycrystalline yield stress, *J. Geophys. Res.*, *84*(B10), 5505–5524, doi:10.1029/JB084iB10p05505.

Farla, R. J. M., H. Kokkonen, J. D. F. Gerald, A. Barnhoorn, U. H. Faul, and I. Jackson (2010), Dislocation recovery in fine-grained San Carlos and sol-gel olivine polycrystals, *Phys. Chem. Miner.*, doi:10.1007/s00269-010-0410-3, in press.

Faul, U. H., and I. Jackson (2007), Diffusion creep of dry, melt-free olivine, *J. Geophys. Res.*, *112*, B04204, doi:10.1029/2006JB004586.

Faul, U. H., J. D. Fitz Gerald, and I. Jackson (2004), Shear wave attenuation and dispersion in melt-bearing olivine polycrystals: 2. Microstructural interpretation and seismological implications, *J. Geophys. Res.*, *109*, B06202, doi:10.1029/2003JB002407.

Frost, H. J., and M. F. Ashby (1982), *Deformation Mechanism Maps*, Pergamon, Oxford, U. K.

Goetze, C. (1978), The mechanisms of creep in olivine, *Philos. Trans. R. Soc. London, Ser. A*, *288*, 99–119, doi:10.1098/rsta.1978.0008.

Goetze, C., and D. L. Kohlstedt (1973), Laboratory study of dislocation climb and diffusion in olivine, *J. Geophys. Res.*, *78*(26), 5961–5971, doi:10.1029/JB078i026p05961.

Goldsby, D. L., and D. L. Kohlstedt (2001), Superplastic deformation of ice: Experimental observations, *J. Geophys. Res.*, *106*(B6), 11,017–11,030, doi:10.1029/2000JB900336.

Heinemann, S., R. Wirth, M. Gottschalk, and G. Dresen (2005), Synthetic [100] tilt grain boundaries in forsterite: 9.9 to 21.5°, *Phys. Chem. Miner.*, *32*, 229–240, doi:10.1007/s00269-005-0448-9.

Hiraga, T., I. M. Anderson, and D. L. Kohlstedt (2003), Chemistry of grain boundaries in mantle rocks, *Am. Mineral.*, *88*, 1015–1019.

Hirth, G., and D. L. Kohlstedt (1995a), Experimental constraints on the dynamics of the partially molten upper mantle: Deformation in the diffusion creep regime, *J. Geophys. Res.*, *100*(B2), 1981–2001, doi:10.1029/94JB02128.

Hirth, G., and D. L. Kohlstedt (1995b), Experimental constraints on the dynamics of the partially molten upper mantle: 2. Deformation in the dislocation creep regime, *J. Geophys. Res.*, *100*(B8), 15,441–15,449, doi:10.1029/95JB01292.

Hirth, G., and D. L. Kohlstedt (2003), Rheology of the upper mantle and the mantle wedge: A view from the experimentalists, in *Inside the Subduction*

Factory, *Geophys. Monogr.*, vol. 138, edited by J. Eiler, pp. 83–105, AGU, Washington, D. C.

Hull, D., and D. J. Bacon (1984), *Introduction to Dislocations*, Butterworth-Heinemann, Oxford, U. K.

Jung, H., and S. I. Karato (2001), Effects of water on the dynamically recrystallized grain size in olivine, *J. Struct. Geol.*, *23*, 1337–1344, doi:10.1016/S0191-8141(01)00005-0.

Jung, H., I. Katayama, Z. Jiang, T. Hiraga, and S. Karato (2006), Effect of water and stress on the lattice-preferred orientation of olivine, *Tectonophysics*, *421*, 1–22, doi:10.1016/j.tecto.2006.02.011.

Karato, S. I. (2008), *Deformation of Earth Materials*, Cambridge Univ. Press, New York.

Karato, S. I., and K.-H. Lee (1999), Stress-strain distribution in deformed olivine aggregates: Inference from microstructural observations and implications for texture development, in *Proceedings of the Twelfth International Conference on Textures and Materials, ICOTOM-12*, vol. 2, edited by J. A. Szpunar, pp. 1546–1555, NRC Res. Press, Ottawa.

Karato, S. I., M. Toriumi, and T. Fujii (1980), Dynamic recrystallization of olivine single crystals during high temperature creep, *Geophys. Res. Lett.*, *7*(9), 649–652, doi:10.1029/GL007i009p00649.

Karato, S. I., M. S. Paterson, and J. D. Fitz Gerald (1986), Rheology of synthetic olivine aggregates: Influence of grain size and water, *J. Geophys. Res.*, *91*(B8), 8151–8176, doi:10.1029/JB091iB08p08151.

Katayama, I., H. Jung, and S. I. Karato (2004), New type of olivine fabric at modest water content and low stress, *Geology*, *32*, 1045–1048, doi:10.1130/G20805.1.

Kirby, S. H., and C. B. Raleigh (1973), Mechanisms of high-temperature, solid-state flow in minerals and ceramics and their bearing on the creep behaviour of the mantle, *Tectonophysics*, *19*, 165–194, doi:10.1016/0040-1951(73)90038-3.

Kochs, U. F., A. S. Argon, and M. F. Ashby (1975), Thermodynamics and kinetics of slip, *Prog. Mater. Sci.*, *19*, 1–291.

Kohlstedt, D. L. (1976), New technique for decorating dislocations in olivine, *Science*, *191*, 1045–1046, doi:10.1126/science.191.4231.1045.

Kohlstedt, D. L. (2006), The role of water in high temperature rock deformation, in *Water in nominally anhydrous minerals*, *Rev. Mineral. Geochem.*, vol. 62, edited by H. Keppler and J. R. Smyth, chap. 16, pp. 377–396, Mineral. Soc. of Am., Washington, D. C.

Kohlstedt, D. L., B. Evans, and S. J. Mackwell (1995), Strength of the lithosphere: Constraints imposed by laboratory experiments, *J. Geophys. Res.*, *100*(B9), 17,587–17,602, doi:10.1029/95JB01460.

Korenaga, J., and S. I. Karato (2008), A new analysis of experimental data on olivine rheology, *J. Geophys. Res.*, *113*, B02403, doi:10.1029/2007JB005100.

Langdon, T. G. (1994), A unified approach to grain boundary sliding in creep and superplasticity, *Acta Metall. Mater.*, *42*, 2437–2443, doi:10.1016/0956-7151(94)90322-0.

Langdon, T. G. (2006), Grain boundary sliding revisited: Developments in sliding over four decades, *J. Mater. Sci.*, *41*, 597–609, doi:10.1007/s10853-006-6476-0.

Lee, K.-H., S. Jiang, and S. i. Karato (2002), A scanning electron microscope study of the effects of dynamic recrystallization on lattice preferred orientation in olivine, *Tectonophysics*, *351*, 331–341, doi:10.1016/S0040-1951(02)00250-0.

Mainprice, D., A. Tommasi, H. Couvy, P. Cordier, and D. J. Frost (2005), Pressure sensitivity of olivine slip systems and seismic anisotropy of Earth's upper mantle, *Nature*, *433*, 731–733, doi:10.1038/nature03266.

Mei, S., and D. L. Kohlstedt (2000), Influence of water of plastic deformation of olivine aggregates: 2. Dislocation creep regime, *J. Geophys. Res.*, *105*(B9), 21,471–21,481, doi:10.1029/2000JB900180.

Michibayashi, K., and D. Mainprice (2004), The role of pre-existing mechanical anisotropy on shear zone development within oceanic mantle lithosphere: An example from the oman ophiolite, *J. Petrol.*, *45*, 405–414, doi:10.1093/petrology/egg099.

Mitchell, T., J. Hirth, and A. Misra (2002), Apparent activation energy and stress exponent in materials with a high Peierls stress, *Acta Mater.*, *50*, 1087–1093, doi:10.1016/S1359-6454(01)00409-8.

Newman, J., W. M. Lamb, M. R. Drury, and R. L. M. Vissers (1999), Deformation processes in a peridotite shear zone: Reaction-softening by an h2o deficient, continuous net transfer reaction, *Tectonophysics*, *303*, 193–222, doi:10.1016/S0040-1951(98)00259-5.

Nicolas, A. (1978), Stess estimates from structural studies in some mantle peridotites, *Philos. Trans. R. Soc. London, Ser. A*, *288*, 49–57, doi:10.1098/rsta.1978.0005.

Paterson, M. S. (1990), Rock deformation experimentation, in *The Brittle-Ductile Transition in Rocks*, *Geophys. Monogr. Ser*, vol. 56, edited by A. G. Duba, pp. 187–194, AGU, Washington, D. C.

Pearson, D. G., D. Canil, and S. B. Shirey (2003), Mantle samples included in volcanic rocks: Xenoliths and diamonds, in *Treatise on Geochemistry*, vol. 2, pp. 171–275, Elsevier, Amsterdam.

Phakey, P., G. Dollinger, and J. Christie (1972), Transmission electron microscopy of experimentally deformed olivine crystals, in *Flow and Fracture of Rocks*, *Geophys. Monogr. Ser*, vol. 16, edited by H. C. Heard et al., pp. 117–138, AGU, Washington, D. C.

Pieri, M., L. Burlini, K. Kunze, I. Stretton, and D. L. Olgaard (2001), Rheological and microstructural evolution of Carrara marble with high shear strain: Results from high temperature torsion experiments, *J. Struct. Geol.*, *23*, 1393–1413, doi:10.1016/S0191-8141(01)00006-2.

Poirier, J.-P. (1985), *Creep of Crystals: High-Temperature Deformation Processes in Metals Ceramics and Minerals*, Cambridge Univ. Press, New York, doi:10.1017/CBO9780511564451.

Raleigh, C. B. (1968), Mechanisms of plastic deformation of olivine, *J. Geophys. Res.*, *73*(16), 5391–5406, doi:10.1029/JB073i016p05391.

Raterron, P., E. Amiguet, J. Chen, L. Li, and P. Cordier (2009), Experimental deformation of olivine single crystals at mantle pressures and temperatures, *Phys. Earth Planet. Inter.*, *172*, 74–83, doi:10.1016/j.pepi.2008.07.026.

Renner, J., and B. Evans (2002), Do calcite rocks obey the power law creep equation?, in *Deformation Mechanisms, Rheology and Tectonics: Current Status and Future Perspectives*, edited by S. De Meer et al., *Geol. Soc. Spec. Publ.*, 200, 293–307.

Renner, J., B. Evans, and G. Siddiqi (2002), Dislocation creep of calcite, *J. Geophys. Res.*, *107*(B12), 2364, doi:10.1029/2001JB001680.

Ricoult, D. L., and D. L. Kohlstedt (1983), Structural width of low-angle grain boundaries in olivine, *Phys. Chem. Miner.*, *9*, 133–138, doi:10.1007/BF00308370.

Rutter, E. H. (1974), The influence of temperature, strain rate and interstitial water in the experimental deformation of calcite rocks, *Tectonophysics*, *22*, 311–334, doi:10.1016/0040-1951(74)90089-4.

Rutter, E. H., and K. H. Brodie (2004), Experimental grain size-sensitive flow of hot-pressed Brazilian quartz aggregates, *J. Struct. Geol.*, *26*, 2011–2023, doi:10.1016/j.jsg.2004.04.006.

Schmid, S. M., M. S. Paterson, and J. N. Boland (1980), High temperature flow and dynamic recrystallization in Carrara marble, *Tectonophysics*, *65*, 245–280, doi:10.1016/0040-1951(80)90077-3.

Tommasi, A., D. Mainprice, G. Cannova, and Y. Chastel (2000), Viscoplastic self-consistent and equilibrium-based modeling of olivine lattice preferred orientations: Implications for the upper mantle seismic anisotropy, *J. Geophys. Res.*, *105*(B4), 7893–7908, doi:10.1029/1999JB900411.

Van der Wal, D., P. Chopra, M. Drury, and J. D. Fitz Gerald (1993), Relationships between dynamically recrystallized grain size and deformation conditions in experimentally deformed olivine rocks, *Geophys. Res. Lett.*, *20*(14), 1479–1481, doi:10.1029/93GL01382.

Vissers, R. L. M., M. R. Drury, E. H. HoogerduijnStrating, C. J. Spiers, and D. Van der Wal (1995), Mantle shear zones and their effect on lithospheric strength during continental breakup, *Tectonophysics*, *249*, 155–171, doi:10.1016/0040-1951(95)00033-J.

Warren, J. M., and G. Hirth (2006), Grain size sensitive deformation mechanisms in naturally deformed peridotites, *Earth Planet. Sci. Lett.*, *248*, 438–450, doi:10.1016/j.epsl.2006.06.006.

Zhang, S., S. I. Karato, J. D. Fitz Gerald, U. H. Faul, and Y. Zhou (2000), Simple shear deformation of olivine aggregates, *Tectonophysics*, *316*, 133–152, doi:10.1016/S0040-1951(99)00229-2.

R. Ahlefeldt, R. J. M. Farla, J. D. Fitz Gerald, and I. Jackson, Research School of Earth Sciences, Australian National University, Canberra, ACT 0200, Australia.

U. H. Faul, Department of Earth Sciences, Boston University, 675 Commonwealth Ave., Boston, MA 002215, USA. (ufaul@bu.edu)